Lithium diffusion in Li_2X (X = O, S, and Se): *Ab initio* simulations and inelastic neutron scattering measurements

M. K. Gupta,[1,*] Baltej Singh,[1,2] Prabhatasree Goel,[1] R. Mittal,[1,2,†] S. Rols,[3] and S. L. Chaplot[1,2]
[1]*Solid State Physics Division, Bhabha Atomic Research Centre, Mumbai, 400085, India*
[2]*Homi Bhabha National Institute, Anushaktinagar, Mumbai 400094, India*
[3]*Institut Laue-Langevin, 71 avenue des Martyrs, Grenoble Cedex 9, 38042, France*

(Received 19 March 2019; revised manuscript received 22 April 2019; published 10 June 2019)

We have performed *ab initio* lattice dynamics and molecular-dynamics studies of Li_2X (X = O, S and Se) to understand the ionic conduction in these compounds. The inelastic neutron scattering measurements on Li_2O have been performed across its superionic transition temperature of about 1200 K. The experimental spectra show significant changes around the superionic transition temperature, which is attributed to large diffusion of lithium as well as its large vibrational amplitude. We have identified a correlation between the chemical pressure (ionic radius of X atom) and the superionic transition temperature. The simulations are able to provide the ionic diffusion pathways in Li_2X.

DOI: 10.1103/PhysRevB.99.224304

I. INTRODUCTION

Solid-state batteries are highly sustainable and stable [1,2]. The use of solid electrolyte between the electrodes has enabled one to solve the issue of dendrite formation and leakage of electrolyte [1,3]. An extensive amount of research is underway to predict and design solid ionic conductors with ionic conductivity in the range of that of liquids [4–19]. They are called the superionic conductors and possess an extremely low potential-energy barrier for diffusion in the solid state. Li ion batteries play a very important role in hybrid electric vehicle and large-grid technology [20,21]. Ionic conductivity of electrode and electrolyte materials is an important parameter for the operation of Li-based batteries [20,22]. The diffusion coefficient of Li_2S and Li_2O has been found to be 1.39×10^{-9} m^2/s [23] and 1.19×10^{-9} m^2/s [24] at elevated temperature, respectively. Such compounds find application in photocathodes, fuel cells, power sources, UV space technology appliances, etc.

There is a fundamental difference between the conventional ionic conductors and superionic conductors. Superionic conductors show large ionic conductivity usually >0.1 mS cm^{-1} above certain temperature in contrast to conventional ionic conductor [4–19]. Further, in case of superionic conductors, there is a clear indication of a phase change, either sharp or diffuse, during which conductivity rises [15,25,26]. The superionic transition is classified in two groups, type I and type II. The type-I transition is a first-order transition characterized by a sudden change of the diffusion coefficient above the transition temperature, while in type-II superionic conductor the diffusivity changes continuously. Li ion diffuses while the host lattice (oxygen/sulfur/selenium) ions constitute the rigid framework. The mechanism and rate of Li diffusion through Li-based battery materials have been studied extensively [21,27,28]. In addition, different strategies have been proposed to increase the carrier concentration and mobility in order to improve the Li ion conductivity in solid-state materials [28,29].The search of superionic conductor $Li_{10}GeP_2S_{12}$ by Kamaya *et al.* [14] triggered the attention of material scientists to activate the field of Li and Na superionic conductors. Many oxides and sulfide compounds like $Li_7La_3Zr_2O_{12}$ [6] and sodium (Na) Super Ionic CONductor (NASICON) [30,31], discovered later, were found to exhibit high Li ionic conductivity of $\sim 1-10$ mS cm^{-1} at room temperature, and low activation energy, $\sim$0.2–0.3 eV.

Above the superionic transition temperature, diffusion of a particular species of ions occurs inside a solid, often referred to as a sublattice melting, which may be accompanied by softening of the related phonon modes [32–34]. The eigenvector of these soft modes can be related to the directions of ionic diffusion and hence might suggest the minimum-energy pathways for diffusion [34,35]. The static energy transition calculations along those specific pathways can be used for estimation of the activation energy barrier. Understanding the role of anharmonic phonon modes responsible for the diffusion mechanism is very important for improving ionic conduction.

Extensive experimental and theoretical studies have been carried out to understand the structure and diffusion behavior of superionic compounds [17,36,37]. X-ray diffraction, neutron scattering, dielectric- and NMR spectroscopic techniques proved useful for characterizing the structure and ionic conduction in the battery materials [38–41]. However, the underlying mechanism of atomic-level behavior of atoms giving rise to these properties can be studied well by *ab initio* computational techniques [29,42]. Recent advancement in computer hardware has enabled material scientists to perform *ab initio* molecular dynamics on hundreds of atoms. The

*mayankg@barc.gov.in
†rmittal@barc.gov.in

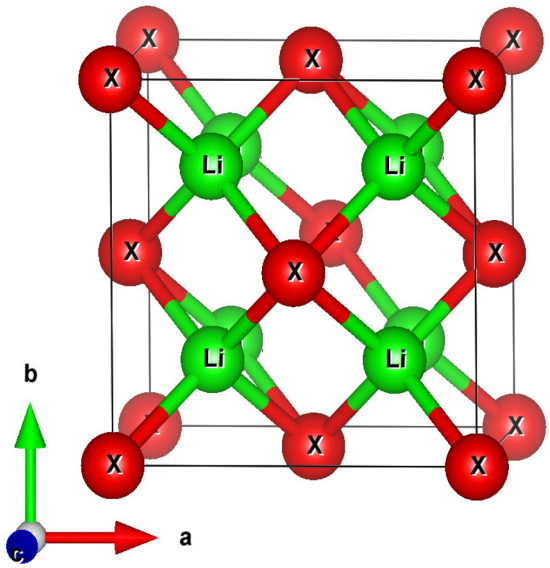

FIG. 1. The crystal structure of Li_2X(X = O, S and Se) at ambient condition. The red sphere are X (X = O, S and Se) atoms and green sphere represent Li.

calculations have been successfully applied to many superionic conductors to predict and understand anisotropic diffusion pathways and correlated ionic movements [3,15,29,43,44]. Quasielastic neutron scattering studies on diffusion in Li_2S by Altorfer *et al.* [23] discuss two models for Li hopping in the fast ion conduction phase, namely (i) Li jumping between vacancy and a regular site; and (ii) Li jumping between interstitial and regular sites.

Li-based compounds are of special interest due to their applications in Li-based batteries. Simple fluorite/antifluorite structured compounds mostly exhibit superionic transition. At ambient conditions, Li_2S and Li_2O occur in the antifluorite structure with space group O_h^5 ($Fm3m$) [45,46]. Sulfur and oxygen ions are arranged in a fcc sublattice with lithium ions occupying the tetrahedral sites. The compounds undergo pressure-induced transformation from antifluorite to anticottunite phase at high pressure of 13 GPa (Li_2S) and 45 GPa (Li_2O), respectively [47,48]. Copious simulation studies have been carried out on similar fluorites and antifluorites like CaF_2, UO_2, Li_2O, etc. We have previously carried out extensive studies on the superionic property of Li_2O using theoretical simulations to deduce the possible easy direction for the diffusion of lithium [33]. Several glassy solutions of Li_2S and Li_2O have been studied extensively in $Li_2S - P_2S_5$ [49] and $Li_2O - B_2O_3 - SiO_2$ with search for increased ionic conduction in mind [50]. There are indirect Raman [51] studies which indicate that Li_2S shows fast ion conduction at 850 K. There are no reported data on measurement of diffusion coefficient in the compounds. A thorough investigation of temperature-dependent Li ion conductivity studies in Li_2S is clearly needed.

Here we focus our study to investigate the factors which trigger superionic behavior in these Li-based antifluorite structures. The compounds Li_2X crystallize in the antifluorite structure (space group 225, $Fm-3m$). At ambient condition (Fig. 1) the Li atoms occupy the 8c Wyckoff positions, while X(O, S, and Se) atoms occupy the 4a sites. We have chosen Li_2O, Li_2S, and Li_2Se compounds. These are fast ion conductors exhibiting high ionic conductivity at high temperatures well below the melting temperature. Due to large electronic band gap they may find applications in battery material as electrolyte. But, the thermodynamic and mechanical stability of electrolyte is another factor to be taken care of. The mechanical and thermodynamical stabilities are governed by the phonons in crystalline materials. Here, in this work our aim is to understand the role of lattice dynamics in diffusion of Li ion and the stability of crystal in these fluorite structures. Our main impetus in this work is to carry out a comprehensive study of vibrational properties of the compounds along with high-temperature molecular-dynamics simulations to understand the superionic conduction mechanism in Li_2O, Li_2S, and Li_2Se. Our experimental neutron scattering studies reveal the behavior of Li sublattice of Li_2O with increasing temperatures. This would give us an idea of the possible role of phonons in the high-temperature behavior of these compounds. In this manner, we would be able to throw some light on the mechanism of diffusion in Li_2O, Li_2S, and Li_2Se.

II. EXPERIMENTAL

The polycrystalline samples of Li_2O were purchased from Sigma-Aldrich. The inelastic neutron scattering experiment on Li_2O is carried out using the IN4C spectrometer at the Institut Laue Langevin, France. The spectrometer is based on the time-of-flight technique and is equipped with a large detector bank covering a wide range of about 10° to 110° of scattering angle. The inelastic neutron scattering measurements were performed at several temperatures from 300 to 1273 K. About 2 cc of polycrystalline sample of Li_2O has been used for the measurements. For these measurements we have used an incident neutron wavelength of 2.4 Å (14.2 meV) in neutron energy gain setup. In the incoherent one-phonon approximation, the measured scattering function $S(Q,E)$, as observed in the neutron experiments, is related [52–54] to the phonon density of states $g^{(n)}(E)$ as follows:

$$g^{(n)}(E) = A\left\langle \frac{e^{2W(Q)}}{Q^2} \frac{E}{n(E,T) + \frac{1}{2} \pm \frac{1}{2}} S(Q,E) \right\rangle, \quad (1)$$

$$g^{n}(E) = B \sum_k \left\{ \frac{4\pi b_k^2}{m_k} \right\} g_k(E), \quad (2)$$

where the "+" or "–" signs correspond to energy loss or gain of the neutrons, respectively, and where $n(E,T) = [\exp(E/k_BT) - 1]^{-1}$. A and B are normalization constants and b_k, m_k, and $g_k(E)$ are, respectively, the neutron scattering length, mass, and partial density of states of the kth atom in the unit cell. The quantity between $\langle\rangle$ represents suitable average over all Q values at a given energy. $2W(Q)$ is the Debye-Waller factor averaged over all the atoms. The weighting factors $4\pi b_k^2/m_k$ for various atoms in the units of barns/amu are 0.1974 and 0.2645 for Li and O, respectively. The values of neutron scattering lengths for various atoms can be found from Ref. [55].

III. COMPUTATIONAL DETAILS

The lattice- and molecular-dynamics simulations of Li_2X (X = O, S, and Se) are performed in the cubic phase (space group $Fm-3m$) using *ab initio* density-functional theory as implemented in the VASP software [56,57]. A supercell of (2 × 2 × 2) dimension, which consists of 96 atoms, has been used in the computations. In the lattice dynamics calculations, the required force constants were computed within the Hellmann-Feynman framework, on various atoms in different configurations of a supercell with ($\pm x$, $\pm y$, $\pm z$) atomic displacement patterns. An energy cutoff of 900 eV was used for plane-wave expansion. The Monkhorst-Pack method [58] is used for k-point generation with a 2 × 2 × 2 k-point mesh. The valence electrons of various atoms in Li_2X considered in total energy calculations are $1s^2 2s$ [1] for Li atom (3 valence electrons in Li atom), while ns^2np^4 for X atoms (6 electrons in X atoms, n = 2, 3, and 4 for O, S, and Se, respectively). The convergence breakdown criteria for the total energy and ionic force loops were set to 10^{-8} eV and 10^{-4} eV Å^{-1}, respectively. We have used PHONOPY software [59] to obtain the phonon frequencies in the entire Brillouin zone, as a subsequent step to density-functional theory total-energy calculations.

The thermal expansion behavior has been computed under the quasiharmonic approximation [60]. Each phonon mode of energy E_{qj}(jth phonon mode at point q in the Brillouin zone) contributes to the thermal expansion coefficient, which is given by the following relation:

$$\alpha_V(T) = \frac{1}{BV_0} \sum_{q,j} C_v(q, j, T)\Gamma_{q,j}, \tag{3}$$

where V_0 is the unit-cell volume, $\Gamma_{q,j}$, is the mode Grüneisen parameter, $C_v(q, j, T)$ is the specific-heat contribution of the phonons of energy $E_{q,j}$. The mode Grüneisen parameter of the phonon of energy $E_{q,j}$ is given as

$$\Gamma_{q,j} = -\left(\frac{\partial \ln E_{q,j}}{\partial \ln V}\right). \tag{4}$$

The molecular-dynamics simulations are carried out in NVT and NVE ensembles. Earlier calculations on pure Li_2S [61] were reported for a supercell size of (2 × 2 × 2) of cubic unit cell, which contains 96 atoms. We have used the same size of supercell in our calculations on Li_2X. The simulations were performed upto 40 ps, with a time step of 1 fs. The temperature in the NVT simulations is attained through a Nosé thermostat [62]. Initially, the structure was equilibrated for 10 ps to attain the required temperature in NVT simulations. Then the production runs up to 40 ps; NVE simulations are performed. Simulations are performed for a series of temperatures from 300 to 1600 K. At each temperature, a well-equilibrated configuration is observed during the 40-ps simulation.

The vibrational density of states has been calculated [63] using Fourier transform of velocity autocorrelation function. The phonon density of states is calculated on 2 × 2 × 2 supercell of the cubic unit cell, which results in averaging of the Brillouin zone on 32 q points. The *ab initio* calculation with larger supercell will be computationally expensive and will give better averaging of the Brillouin zone. However, we found that a 2 × 2 × 2 super cell is able to reproduce the experimental spectrum fairly well. The simulation time of about 40 ps would give energy resolution of ∼0.1 meV in the calculated density of sates, which is quite enough for comparison among Li_2X compounds.

IV. RESULTS AND DISCUSSION

A. Temperature-dependent measurement of phonon spectra

We have performed the inelastic neutron scattering measurements of Li_2O at several temperatures [Fig. 2(a)] from 300 to 1273 K covering the superionic transition at about 1200 K. The room-temperature measurements show well-defined peak structure in the phonon density of states and it disappears at above 973 K below the superionic transition temperature. We have compared the measured phonon density of states at 300 K with the lattice dynamics calculated phonon spectrum [Fig. 2(b)]. The neutron-weighted phonon density of states show peaks at about 30, 50, 65, and 90 meV. Partial contributions from Li and O atoms to the total density of states are also shown. We can see that both Li and O have almost equal contribution in entire spectrum except at about 50–70-meV regime, where Li has dominating contribution. The calculated total neutron-weighted phonon density of states is in good agreement with measurements [Fig. 2(b)]. As temperature is increased to 773 K, the peak at about 50 meV in the phonon density of states is found to shift toward lower energy with respect to the spectrum at 300 K [Fig. 2(a)]. This could well be understood by comparing the partial contribution of lithium and oxygen with the measured phonon density of states. At higher temperature the mean-squared amplitude of Li vibration becomes very large, and their contribution to the total density of states [$g_k(E)e^{-Q^2u^2}$] becomes smaller and contribution from oxygen will dominate. Further, at higher temperature, the phonon spectrum of oxygen sublattice softens due to large thermal expansion of Li_2O. On further increase of temperature to 973 K and above, the measured spectra seem like a broad envelope; this could be due to large mean-square displacement of Li and O as well as diffusion of Li. The superionic temperature of Li_2O is 1200 K (∼927 °C) [64]. The neutron scattering data indicate significant increase in the anharmonicity of the phonons around 973 K. This may happen at a temperature that is somewhat lower than the superionic transition temperature.

At high temperature, where the anharmonicity of vibrations becomes significant, we need to perform molecular-dynamics simulation to evaluate the phonon spectrum. In Fig. 3, we have shown the calculated phonon density of states from molecular-dynamics simulations at 300 and 1200 K and compared it with the measurements. The room-temperature calculated phonon density of states reproduces the peak features close to the measurements, whereas at 1200 K the spectrum gets significantly broadened. The fair agreement between the calculation and measurements validates the robustness of the method and can be utilized for further microscopic analysis. The phonon density of states calculations performed using both lattice dynamics [Fig. 2(b)] and molecular-dynamics simulations (Fig. 3) show a fair agreement and indicate a fair degree of convergence.

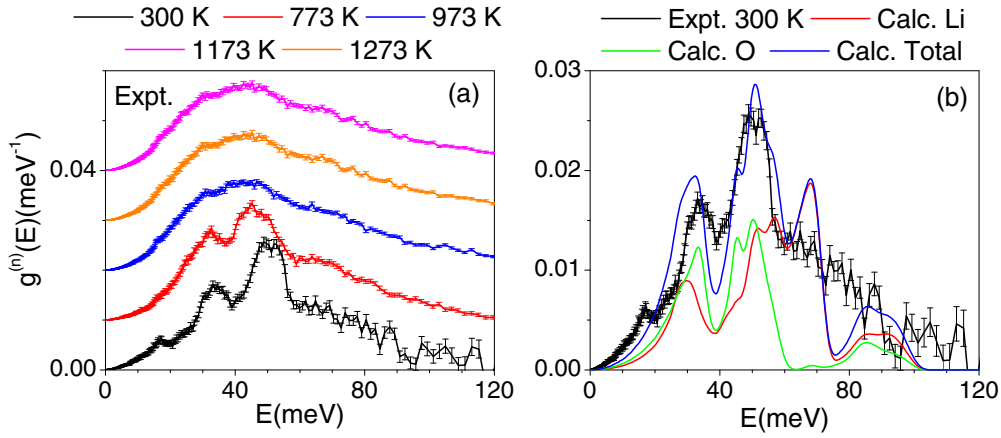

FIG. 2. (a) Measured temperature dependence of inelastic neutron scattering spectra of Li_2O.For clarity the experimental data at various temperatures are shifted vertically.(b) The calculated neutron-cross-section weighted phonon density of states using lattice dynamics and compared with the measurement at T = 300 K.

B. Thermodynamics behavior of Li_2X (X = O, S, and Se) from lattice dynamics

There has been several studies on fluorite structures as well as other superionic conductors [19,65–70] to address the importance of phonon softening at superionic transition. These studies include the calculations performed by *ab initio* molecular-dynamics approach to overcome the limitation of quasiharmonic approximation of lattice dynamics. In Fig. 4, we have computed the phonon-dispersion relation of Li_2X (X = O, S, and Se) along various high-symmetry directions and compared with the available measurements in Li_2O and Li_2S [71,72]. The phonon-dispersion relation in Li_2O shows that along the (001) direction one of the optic branches shows large dispersion and at the zone-boundary point the energy of this optic phonon branch is lowest (24 meV). Interestingly the eigenvector of this phonon mode shows displacement of lithium atoms while oxygen's remains at rest, which is linked to phonon instability in Li_2O at high temperatures [33]. However in Li_2S and Li_2Se, the same optic branch shows less dispersion behavior and also the phonon mode energy at the

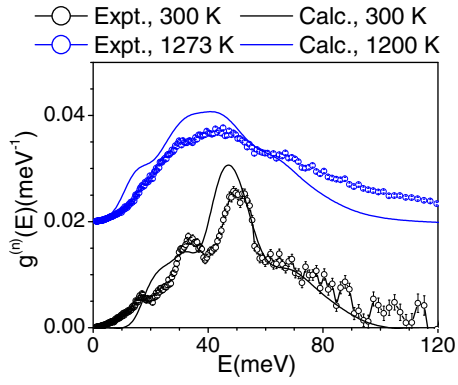

FIG. 3. The calculated and experimental neutron weighted phonon density of states at 300 and 1200 K. The phonon spectra have been calculated using ab-initio molecular dynamics simulations.

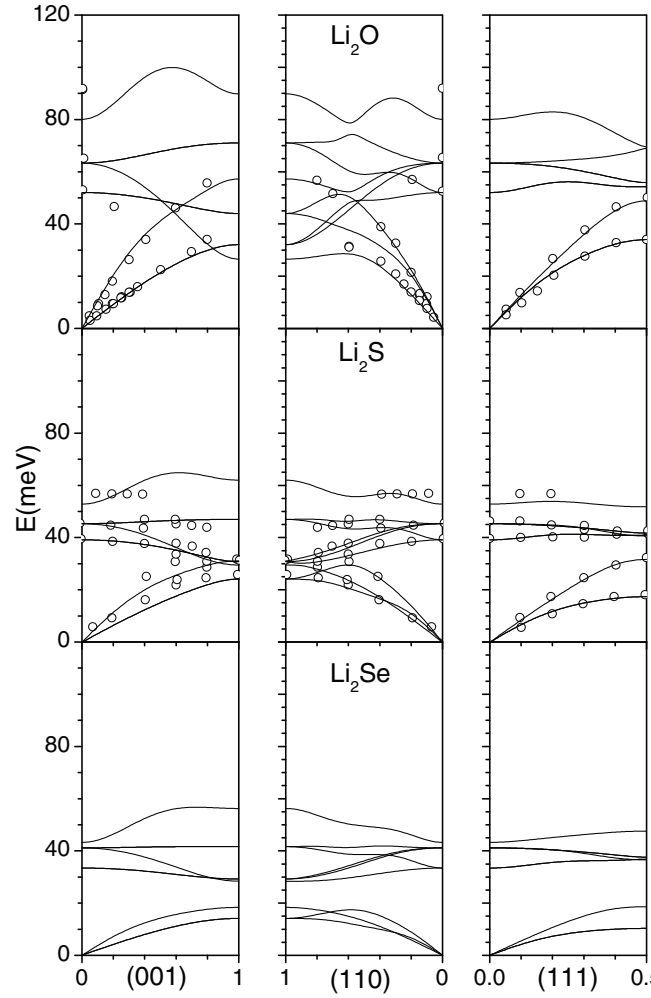

FIG. 4. The calculated dispersion relation of Li_2X(X = O, S and Se) along various high symmetry direction in Brillouin zone and compared with the available measurements. The solid lines and open circles correspond to the calculations and experimental data [71,72].

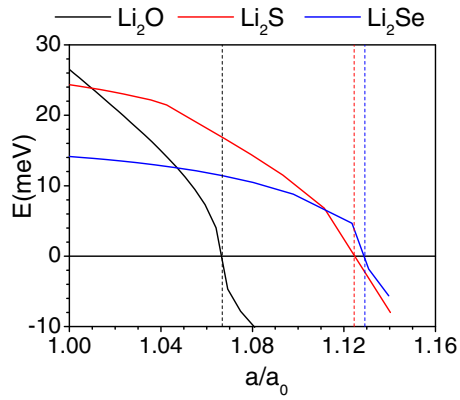

FIG. 5. Cell parameter dependence of zone boundary phonon mode at (001) in Li_2X (X = O, S and Se).

zone boundary is higher (30 meV) than that in Li_2O (24 meV). This change may be due to softer host structure of Se and S as compared with O host structure as well as the difference in interaction strength of Li with host lattice. It seems that as we increase the size of the cation X (X = O, S, and Se) the dispersion of the optic branch becomes less dispersive.

In our previous work, we have shown [33] that with change in volume the optic mode at zone boundary becomes unstable when the volume increases to the value close to superionic transition temperature, indicating that volume-driven instability of the phonon mode may initiate the lithium diffusion in Li_2O at higher temperature. We have calculated the volume dependence of zone-boundary phonon mode at (001) in other two compounds (Fig. 5). We can see that the percentage lattice parameter "a" change required for phonon instability in Li_2O is about 6.6%; however, in Li_2S and Li_2Se this is as large as 12.5 and 12.9%, respectively, which is not possible. Such expansion of the lattice would result in melting of the compound. As mentioned above, it seems that in case of Li_2O the lowest optical branch shows the large dispersion and the zone-boundary mode of this branch destabilizes at higher temperature, while in the other two compounds the same branch does not show significant dispersion and even at high temperature the zone-boundary mode of the same may not destabilize. Further, due to lower Li band center and soft host structure, a significant number of lithium are vibrating with higher amplitude and may lead to diffusion in Li_2S and Li_2Se at high temperature.

Recent work by Cazorla *et al.* [69] showed that the instability predicted by lattice dynamics at unit-cell volume at superionic regime stabilizes due to strong temperature-driven anharmonicity and phonon-phonon coupling. The anhamonicity due to higher temperature and lattice defects plays an important role in stabilizing the superionic phase which can be treated appropriately using molecular dynamics, while lattice dynamics formalism does not account for these effects. The correlation between the center of phonon energy distribution, i.e., band center and potential of ionic diffusion is discussed in great detail by Muy *et al.* [8]. The authors showed a correlation between Li band center and barrier energy for Li migration from lattice dynamics and nudged elastic band (NEB) calculations. However, later Sagotra *et al.* [73] have shown that Li activation energies as estimated from lattice dynamics and NEB methods underestimate the actual activation energy due to the neglect of temperature effects, and harmonic approaches.

In Fig. 6, we have shown the calculated partial and total density of states of Li_2X (X = O, S, and Se) compounds. The Li and O partial density of states in Li_2O extend in the entire spectrum range up to 100 meV. However, in Li_2S the spectral range extends up to 50 meV only. The lower part of the spectrum up to 30 meV is dominated by S, while higher-energy spectrum above 30 meV has contributions mainly from Li. In Li_2Se, the contributions due to Li and Se are well separated. The contributions due to Se and Li are below and

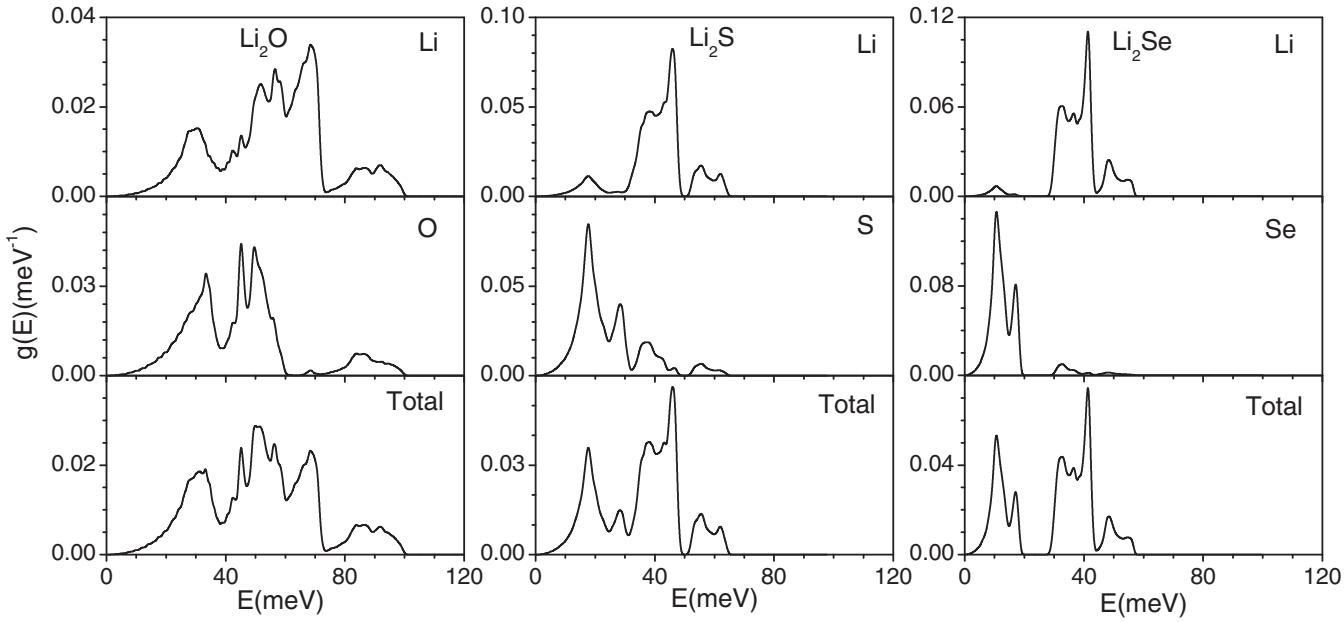

FIG. 6. The lattice dynamics calculated total density of states and partial density of states of Li and X in Li_2X(X = O, S, Se) compounds.

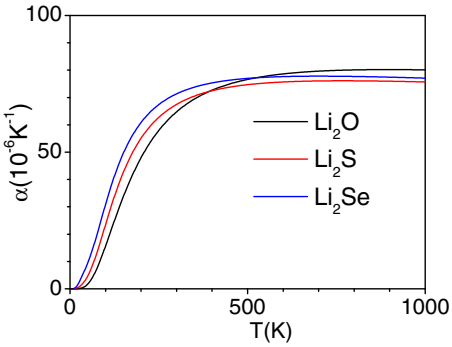

FIG. 7. The calculated volume thermal expansion coefficient of Li_2X(X = O,S and Se) compounds.

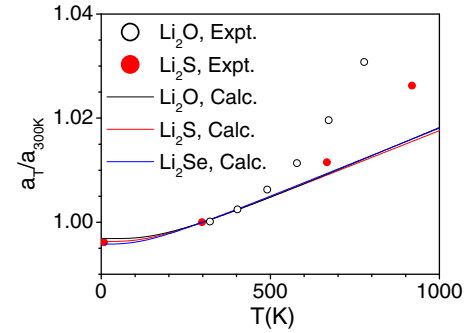

FIG. 8. The calculated and experimental [74,75] fractional change in lattice parameter with temperature of Li_2X (X = O,S and Se).

above 20 meV, respectively. The band center of the peaks of Li phonon density of states in various compounds are at 57, 42, and 38 meV in Li_2O, Li_2S, and Li_2Se, respectively, and for O, S, and Se the vibrations are centered at about 45, 21, and 12 meV, respectively.

It can be seen that the Li band center moves towards lower-energy regime as we go from Li_2O to Li_2Se, which indicates decrease in bonding strength of Li atom with host, which is good for better ionic conductivity, while the shift of the band center of anion (X = O, S, and Se) indicates the poor stability of host structure, i.e. the mechanical stability of O sublattice is good while that of Se sublattice is least among the three compounds. This suggests that from the stability point of view Li_2O is best among the three; however, from the diffusion point of view Li_2Se is better than other two. So there is a trade-off between host stability and ionic conduction. This suggests that for a better electrolyte/electrode one can play with stoichiometry of O, S, and Se to optimize the property in a mixture of all these compounds. By doing this, one may achieve the low-energy Li spectrum and moderate host stability.

The fluorite structure compounds are also known for their high thermal expansion coefficient. The volume thermal expansion coefficient of Li_2X compounds has been computed under quasiharmonic approximation (Fig. 7). The calculated coefficient of volume thermal expansion at 400 K is $\sim 80 \times 10^{-6}\,K^{-1}$ in all three compounds. However, at lower temperature the Li_2Se shows the largest thermal expansion among all Li_2X (X = O, S, and Se). The lower band center of host element X(O, S, and Se) in Li_2Se and Li_2S in comparison to Li_2O facilitated the host structure to expand at much lower temperature. The comparison between the experimental [74,75] and calculated thermal expansion behavior of Li_2O and Li_2S is shown in Fig. 8. The deviation between experiments and calculations increases above 600 K, which indicates that at high temperature explicit anharmonic effects [60] due to large thermal amplitude of atoms are important. The quasiharmonic calculations of thermal expansion only consider the change in phonon energies with volume.

C. Estimate of barrier energy for lithium migration

In order to get an estimate of barrier energy for lithium migration from one tetrahedral site to another tetrahedral site we have performed the energy-barrier calculations along various high-symmetry directions using NEB methods. These calculations are performed for Li movements along the [100], [110], and [111] directions. A number of structural images are generated along the initial path of diffusion which is then optimized to obtain the actual diffusion pathways and activation energy barrier. The calculated activation energy barrier and final optimized pathways are shown in Fig. 9. It can be seen that the diffusion pathway along the [100] direction in all Li_2X compounds is nearly straight. We found

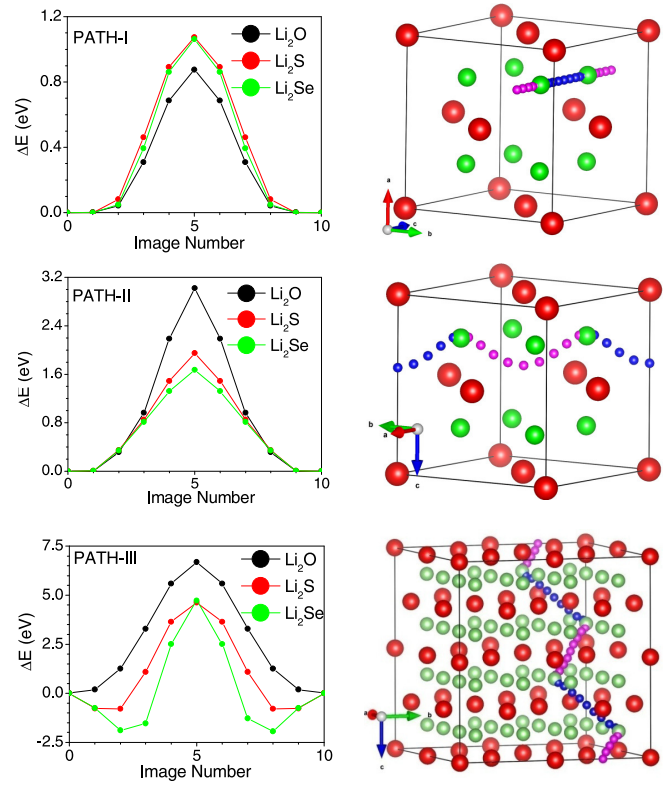

FIG. 9. The calculated activation energy barrier for Li diffusion along various directions in the unit cell of Li_2X(X = O, S, Se). PATH-I (along [100]), PATH-II (along [110]), and PATH-III (along [111])corresponds to correlated movement of 2, 2 and 4 Li atoms, respectively. PATH-III calculation are done in a $2 \times 2 \times 2$ supercell. At ambient conditions lithium atoms occupy only tetrahedral sites (green spheres) in the crystal. The X (= O, S, Se) atoms are shown by red spheres.

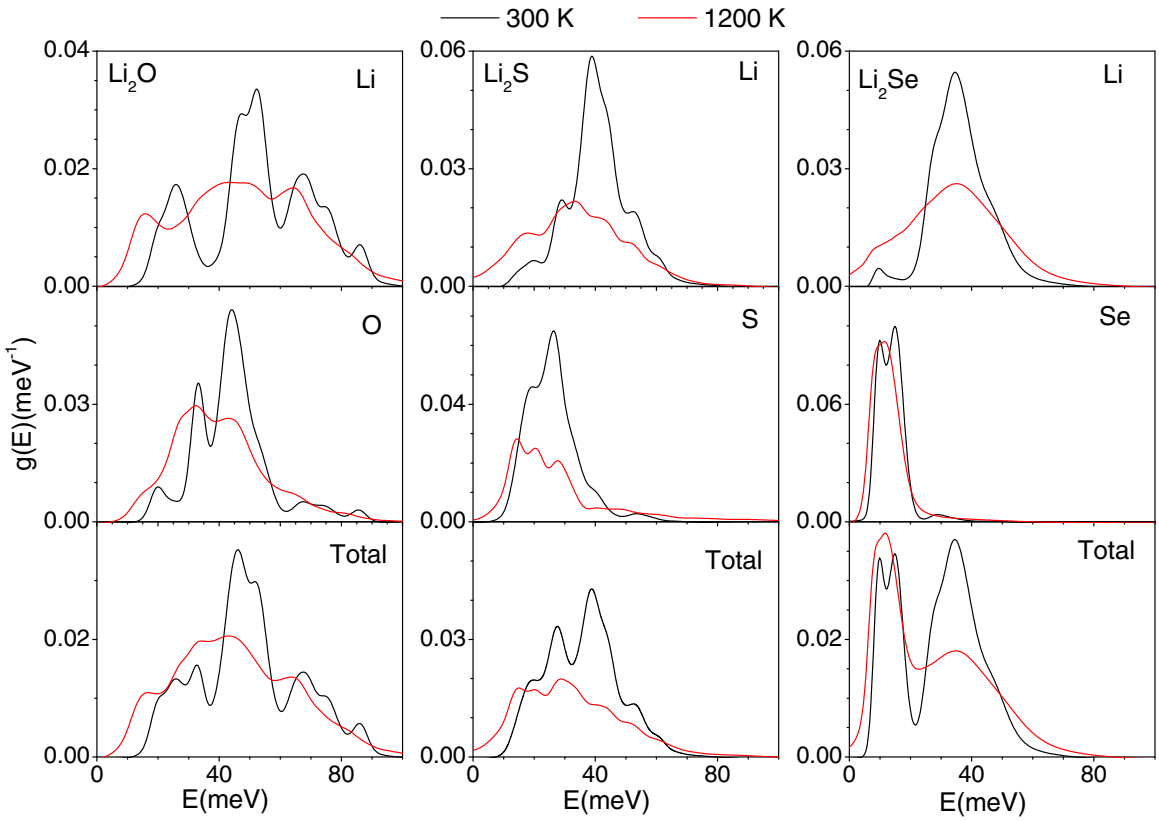

FIG. 10. The calculated phonon spectrum of Li and X in Li_2X(X = O,S and Se) compounds using molecular dynamics simulation at 300 K and above superionic transition temperature (T = 1200 K).

that activation energy is least for Li_2O compound along [100]. This implies that mechanism for Li diffusion along [100] is more probable in Li_2O in comparison to that for Li_2S and Li_2Se.

The second path for Li diffusion along the [110] direction shows (Fig. 9) curved diffusion pathway. The activation energy barriers for Li diffusion along this direction show higher barrier for Li_2O than that for Li_2S and Li_2Se. This may arise from the more open channel along [110] in Li_2Se and Li_2S for Li diffusion than that in Li_2O due to larger size of Se and S than O. The diffusion of Li along [111] seems (Fig. 9) to be prohibited for Li_2O due to a large barrier energy. However, in case of Li_2S and Li_2Se, there is a significant attractive potential in a smaller vicinity towards the ⟨111⟩ direction and thereafter it shows a large barrier. Such potentials might lead to a possibility of complex diffusion pathways. Hence to examine other possibilities of Li migration, we have performed the analysis of Li trajectory obtained from molecular-dynamics simulation (Sec. IV D).

Our molecular-dynamics simulations show very different and interesting pathways for diffusion in these compounds. The interesting thing to note in these calculations (Fig. 9) is the dip along [111] directions at (¼ ¼ ¼) position of Li for Li_2S and Li_2Se. This may be arising from the possibility of available jump sites at these intervening positions. The possibility of these intervening jumps increases as we go from Li_2O to Li_2Se. Recent work by Sagora *et al.* [73] has also found significant difference in barrier-energy estimation from NEB and molecular-dynamics simulations.

D. Thermodynamics properties of Li_2X (X = O, S, and Se) from molecular dynamics

The above discussion is based on the lattice dynamics calculations which are performed at 0 K and the thermodynamic behaviour is obtained under the quasiharmonic approximation. The lattice dynamics provide us the estimate of the phonon properties (density of states, elastic properties etc) of materials and help us to understand the difference in material properties at 0 K. However, at higher temperature when system is close to some instability or transition (like superionic transition in this case), the effect of anharmonicity significantly dominates and cannot be accurately represented by quasiharmonic effects. Hence in order to account the anharmonic effect and understand the Li diffusion and its consequences on inelastic neutron scattering spectrum we have carried out the *ab-intio* molecular dynamics simulation. The calculations are performed at various temperatures ranging from room temperature to across the superionic transition temperature of Li_2X compounds.

We have first looked at the effect of temperature on the vibrational spectrum i.e. phonon density of states of various elements in Li_2X(Fig. 10). We found that at room temperature the spectrum of Li and X(O,S and Se) shows sharp peak features. However, at 1200 K(above the superionic temperature) the Li spectrum becomes very broad and at zero energy there is finite density of states, which is a signature of diffusion. The magnitude of this shift is maximum in Li_2Se, which is again consistent with our lattice dynamics result that Li ion

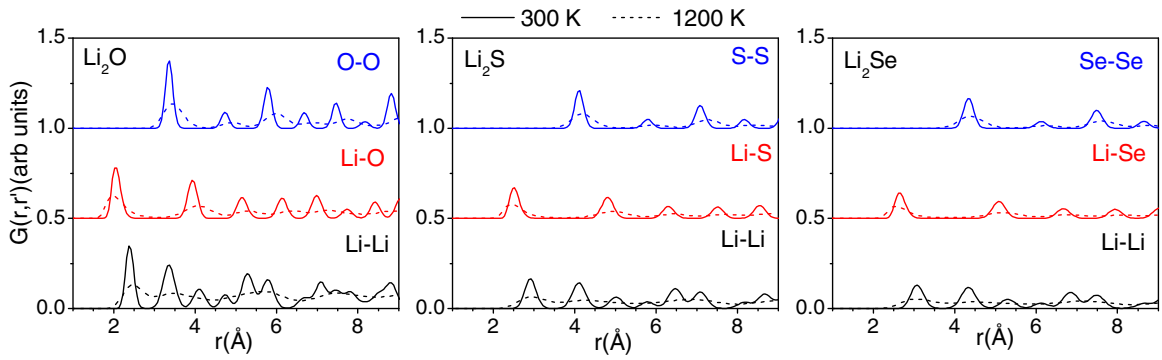

FIG. 11. The calculated pair correlation function between various pairs of atom in Li_2X(X = O,S and Se) at T = 300 (solid line) and T = 1200 K (dashed line).

diffusion is much easier in Li_2Se in comparison to the other two compounds. Further, we could see that the density of states of host element, i.e. X(X = O,S and Se) also broaden with temperature but lesser in magnitude than that of Li. The peak like structure in the spectra still persists above the superionic transition temperature, indicating that the atoms remain intact with the lattice most of the time.

Further, diffusion of Li occurs in the lattice at high temperature. Its local environment keeps changing with time, and this will give rise to broadening in the pair distribution function(PDF) of Li-X(X = O,S and Se) and Li-Li averaged over space and time. We have calculated (Fig. 11) the pair distribution function for various pair of atoms in Li_2X(X = O,S and Se). We could see that at room temperature, the PDF of all pairs of atoms show sharp peaks at finite positions. This is due to the fact that at room temperature the local environments of all the atoms are almost invariant with time. We find that the PDF of Li-Li and Li-X pairs at higher temperature of 1200 K clearly show only first two peaks(i.e. up to second neighbor distance) and the peaks at higher inter-atomic distance get broadened. The PDF between X-X (X = O, S and Se) atoms shows peak like structure up to a few neighbors. Hence the Li sub-lattice in Li_2X melts at superionic temperature, while the host element X(X = O, S and Se) remain intact with the lattice. Similarly at higher temperature the bond angle in the Li_4X polyhedral unit changes with time and it leads to broadening in the angle distribution (Fig. 12).

E. Diffusion in Li_2X (X = O, S and Se) from Molecular Dynamics

In order to design a material with large diffusion coefficient, e.g., electrolyte in battery, one needs to know various channels for diffusion, easy directions of diffusion, activation energy barriers and stability of host structure etc. The mean square displacement is a very important quantity in this regard as it contains most of the information. Hence in order to understand and explain the difference in Li diffusion between various Li_2X(X = O,S and Se) compounds, we have computed the mean square displacement of various atoms as a function of time at different temperatures (Fig. 13). The mean square displacements are averaged over all the atoms of each type. At room temperature the magnitude of mean square displacement of various atoms in Li_2X(X = O,S and Se) is independent with time. Since, the diffusion coefficient is proportional to the time derivative of mean square displacement (MSD), at room temperature the derivative of MSD with time for different element in Li_2X is zero. Hence there is no diffusion at room temperature. As we go to high temperature close to the superionic regime, the mean square displacement of Li atoms in all three compounds starts increasing with time. The calculation of MSD at larger lag time would have poor statistics due to insufficient averaging.

At superionic regime, the host structure is stable and provides discrete sites for Li occupancy, and Li can diffuse through these sites via jump from one site to another; hence

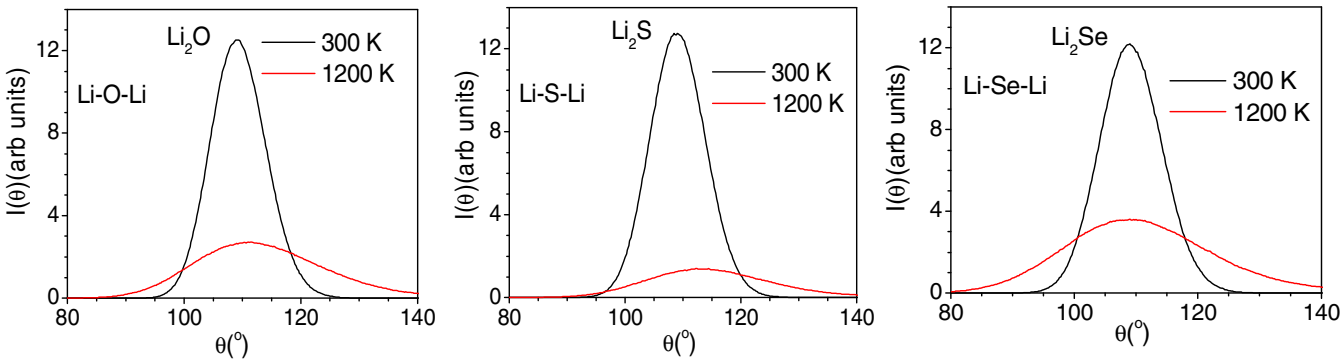

FIG. 12. The calculated angle distribution between Li-X-Li junction in Li_2X(X = O,S and Se) at T = 300 and T = 1200 K averaged over 40 picosecond simulation time and all the atoms in supercell.

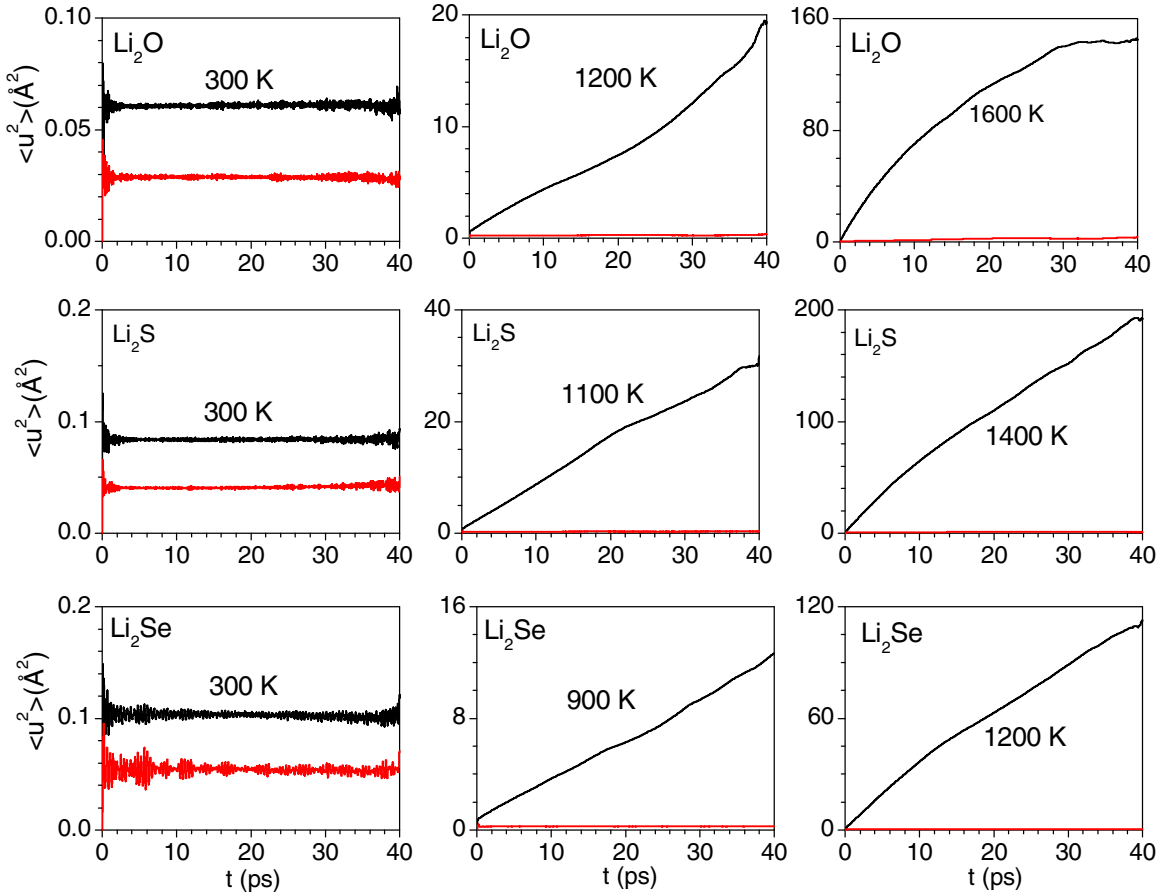

FIG. 13. The calculated mean square displacement of Li and X atom in Li_2X(X = O,S and Se).The black and red solid lines corresponds to Li and X atoms.

the mean square displacement of individual atoms as shown in Fig. 14, shows the step like behaviour. The different jump length is related with different diffusion pathways and their frequency. The number of such jumps will be related to the energy barrier for such diffusion pathways. In all the three compounds we observed that the least jump length is $\sim 4-6\,\text{Å}^2$, which corresponds to Li migration from one tetrahedral site to another tetrahedral site (Fig. 14) directly i.e. along (100) as well as through octahedral site i.e. along (111) direction. The number of such jumps in all the three compounds is very large. This means that diffusion in all three compounds have significant contribution through Li jump along (100) and (111) directions. We have not found any interstitial position for Li occupancy. Hence in the crystalline phase the Li atoms diffuse only via tetrahedral jumps.

In Fig. 15, we have shown the Li trajectory of a few representative Li- ions in Li_2X(X = O,S and Se) compounds. This is useful to understand the minimum energy pathways of Li diffusion in these compounds. Our previous analysis (Figs. 13 and 14) based on time dependence of mean squared displacement showed that only the Li- ions are diffusing while the X(O,S and Se) atoms form a rigid structure even at superionic temperature. Hence for easy visualization and explanation, we have shown (Fig. 15) only Li positions.

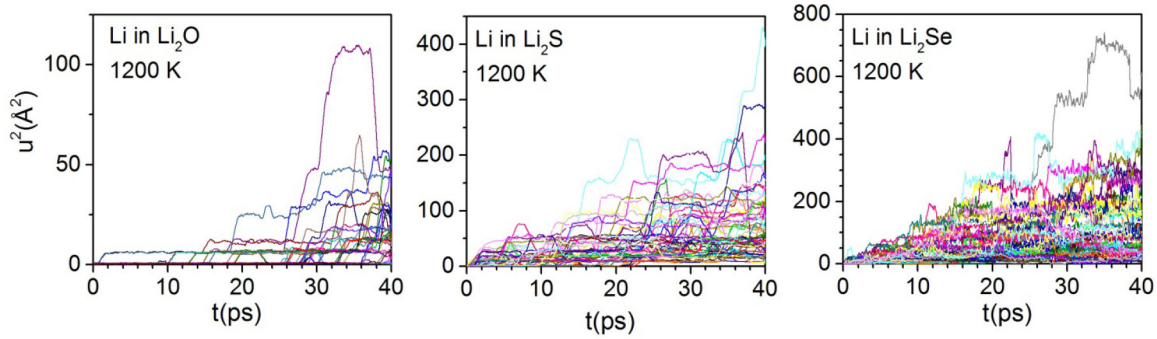

FIG. 14. The calculated displacement of Li atoms in Li_2X (X = O,S and Se) at T = 1200 K.

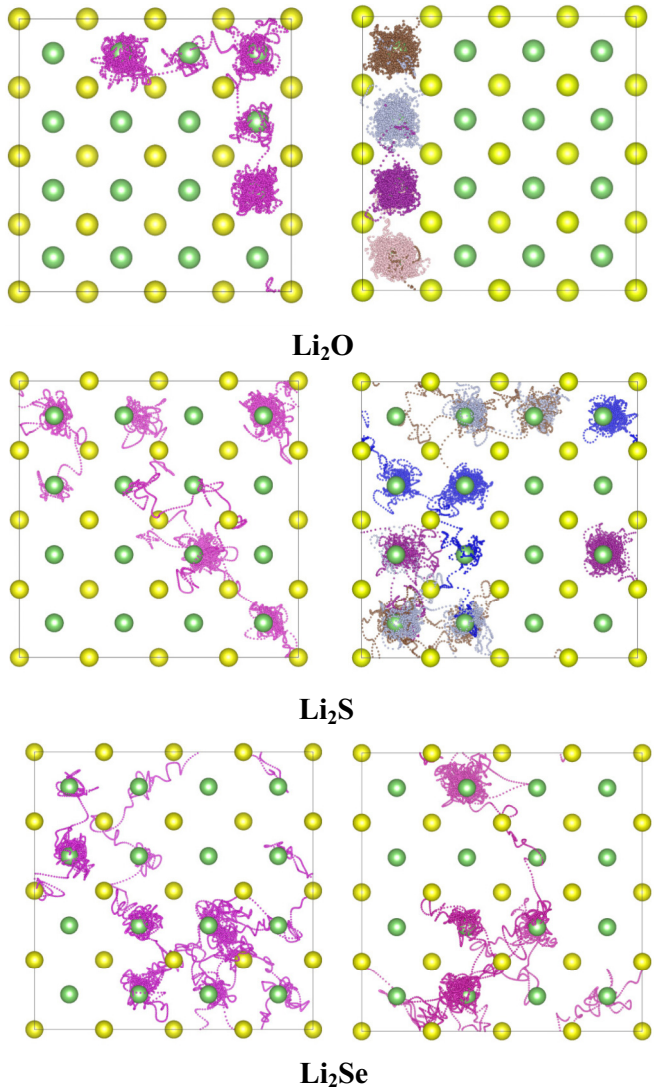

FIG. 15. The calculated trajectories of selected Li atoms at 1200 K in Li_2X (X = O,S and Se) in the a-b plane. Left and Right panel shows the trajectories of two different lithium atoms. At ambient conditions lithium atoms occupy only tetrahedral sites (green spheres) in the crystal. However at higher temperature lithium may also jump from one tetrahedral to another tetrahedral site through the octahedral interstitial sites (yellow spheres). X atoms are not shown. The time dependent positions of Li atoms are shown by colored dots. The calculated trajectories are shown on a $2 \times 2 \times 2$ supercell.

At ambient temperature lithium atoms occupy only tetrahedral sites (green spheres in Fig. 15) in the crystal. However at higher temperature lithium may also jump from one tetrahedral to another tetrahedral site through the octahedral sites (yellow spheres in Fig. 15).The time dependent positions of Li atoms are shown by colored dots in Fig. 15. In case of Li_2O, Li atoms are hoping from one tetrahedral site to another tetrahedral site (green sphere to another green sphere) along (100) or its equivalent directions, i.e. they do not involve any intermediate octahedral position to hop from one tetrahedral site to another site. This is what we have inferred from our lattice dynamics analysis and nudged elastic band energy calculation that the easiest direction for Li migration would be along (100) direction.

Interestingly the story is very different for Li_2S and Li_2Se. Here Li hops (Fig. 15) from one tetrahedral site to another tetrahedral site via octahedral sites as well as via direct jump along (100). But numbers of intermediate octahedral transient states are significant in these two compounds. Further, it is also to be noted that when one Li- hops from one tetrahedral site to another tetrahedral site, the Li at another site simultaneously jumps to another octahedral or tetrahedral site. So there is a cooperative hoping dynamics for Li_2S and Li_2Se. Even in case of Li_2O there is cooperative hoping but it seems that even for cooperative dynamics (100) is most favorable pathway. The Li atoms are located at (0.25 0.25 0.25) and equivalent tetrahedral sites and form LiX_4 tetrahedra. The Li atoms jump from one tetrahedral site to another tetrahedral site in the present study without spending any significant time at any intermediate stage. In some of the jumps, Li atoms pass through an octahedral site (e.g. 0.5 0.5 0.5). This is also inferred from the trajectory plot shown in Fig. 15. In case of Li_2C_2, the Li atoms spend significant time at the octahedral interstitial sites [76], The difference in structure of the two compounds could lead to difference in residence time at the interstitial sites.

The barrier energy which is obtained from nudged elastic band method (Fig. 9) does not give the correct picture of barrier or activation energy for diffusion since NEB diffusion along (111) is prohibited due to large barrier for Li ion migration. Hence in order to correctly predict the diffusion barrier energy one may also need to see the correlated dynamics. Molecular dynamics simulation includes correlated as well as uncorrelated jumps, hence it truly represents the diffusion behaviour.

The isotropic diffusion coefficient is estimated using Einstein law of diffusion i.e. from the time dependence of mean square displacement as given below:

$$D = \langle u^2 \rangle / 6\tau \tag{5}$$

Where, $\langle u^2 \rangle$ is the change in the mean square displacement in time τ.

The mean square displacement (MSD) at time τ is calculated using the following equation [63,73]

$$u^2(\tau) = \frac{1}{N_{\text{ion}}(N_{\text{step}} - N\tau)} \sum_{i=1}^{N_{\text{ion}}} \sum_{j=1}^{N_{\text{step}}-N_\tau} |r_i(t_j + \tau) - r_i(t_j)|^2 \tag{6}$$

Here $r_i(t_j)$ is the position of i^{th} atom at j^{th} time step. N_{step} is total number of simulation steps and N_{ion} is total number of atoms of a particular type in the simulation cell. $N\tau = \tau/\delta t$, where δt is the size of the time step used in the MD simulations.

As noted above, the calculation of MSD at larger lag time would have poor statistics due to insufficient averaging. However, we have used only the linear region in the MSD plots (Fig. 13) to estimate the diffusion coefficients, which gives a fair estimate. The calculated diffusion coefficient as a function of temperature is shown in Fig. 16. One could see that in Li_2O, the diffusion coefficient increases above 1200 K. However, in Li_2S and Li_2Se the diffusion starts at above 1000 K and 900 K respectively. Further in order to correctly

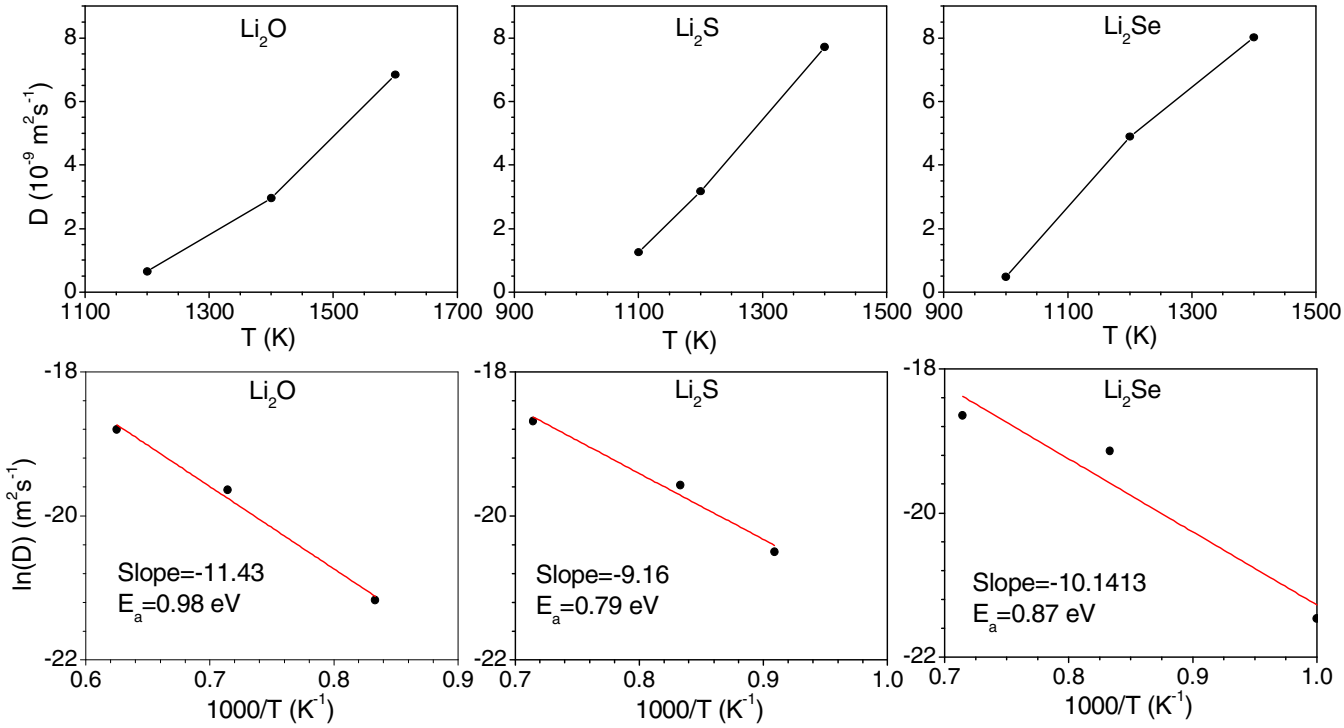

FIG. 16. The calculated diffusion coefficients and activation energy barriersin Li_2X (X = O,S and Se).

estimate the barrier energy from correlated as well uncorrelated dynamics for lithium diffusion in these compounds, we have fitted the temperature dependence of diffusion coefficients with Arhenius relation i.e.

$$D(T) = D_0 \exp(-E_a/K_B T) \tag{7}$$

Here D_0 is the constant factor, K_B is the Boltzmann constant and T is temperature. One can linearize this equation by taking log of it, i.e.,

$$\ln(D(T)) = \ln(D_0) - E_a/K_B T \tag{8}$$

The conductivity measurement on Li_2S showed two different energy barriers of 0.70 eV and 1.52 eV in temperature range below and above 750 K respectively [23], while in Li_2O the values are 1.0 eV and 2.5eV in the temperature range below and above 1200 K respectively [77]. The values of the pre-exponential diffusion factor, D_0 for various compounds are $D_0(Li_2O) = 9.3 \times 10^{-6}\,m^2\,s^{-1}$, $D_0(Li_2S) = 5.6 \times 10^{-6}\,m^2\,s^{-1}$, $D_0(Li_2Se) = 3.94 \times 10^{-6}\,m^2\,s^{-1}$. The high temperature value in the experimental analysis might be due to formations of defects and vacancy at high temperature in the superionic regime. There is no data available for Li_2Se. In Fig 16, we have fitted equation (7) and obtained the value of barrier energy for Li diffusion in all three compounds. The values are 0.98 eV, 0.79 eV and 0.87 eV for Li_2O, Li_2S and Li_2Se respectively. In recent study [78], the authors found a correlation between Li band centre and barrier energy for Li migration on various ionic conductors based on NEB methods, they found that downshifting of lithium phonon band center lowers the migration barrier. However, in the present case Li_2Se has band centre of Li at lowest energy among three compounds but does not have the least barrier energy as estimated from molecular dynamics simulation. Our work shows that temperature dependent anharmonicity inherently incorporated in molecular dynamics simulation is important to estimate the barrier energy.

V. CONCLUSIONS

In this article we have reported extensive *ab-initio* lattice and molecular dynamics simulations aspect to investigate and understand the mechanism of Li diffusion in Li_2X anti-fluorite structures. The uncorrelated or single Li hopping from one tetrahedral to another tetrahedral site favors the ⟨100⟩ path, while ⟨111⟩ direction is least possible. However, correlated diffusion of Li is equally possible along ⟨100⟩ and ⟨111⟩ directions. Hence, for better understanding of pathways, the analysis of single ion dynamics through NEB method is not sufficient. However, one can include various correlated possibilities in the NEB method or use molecular dynamics simulation to evaluate the true barrier energy. The calculated barrier energy of Li_2S is the least among the three compounds; however, from the host stability point of view, Li_2O is a better candidate. By appropriate stoichiometry, one can trade off between these properties.

[1] J. Janek and W. G. Zeier, Nat. Energy **1**, 16141 (2016).
[2] A. L. Robinson and J. Janek, MRS Bull. **39**, 1046 (2014).
[3] W. D. Richards, T. Tsujimura, L. J. Miara, Y. Wang, J. C. Kim, S. P. Ong, I. Uechi, N. Suzuki, and G. Ceder, Nat. Commun. **7**, 11009 (2016).

[4] N. Adelstein and B. C. Wood, Chem. Mater. **28**, 7218 (2016).
[5] Z. Deng, Z. Zhu, I.-H. Chu, and S. P. Ong, Chem. Mater. **29**, 281 (2017).
[6] Y. Chen, E. Rangasamy, C. Liang, and K. An, Chem. Mater. **27**, 5491 (2015).
[7] K. E. Kweon, J. B. Varley, P. Shea, N. Adelstein, P. Mehta, T. W. Heo, T. J. Udovic, V. Stavila, and B. C. Wood, Chem. Mater. **29**, 9142 (2017).
[8] S. Muy, J. C. Bachman, H.-H. Chang, L. Giordano, F. Maglia, S. Lupart, P. Lamp, W. G. Zeier, and Y. Shao-Horn, Chem. Mater. **30**, 5573 (2018).
[9] Y. Sun, K. Suzuki, S. Hori, M. Hirayama, and R. Kanno, Chem. Mater. **29**, 5858 (2017).
[10] W. S. Tang, M. Dimitrievska, V. Stavila, W. Zhou, H. Wu, A. A. Talin, and T. J. Udovic, Chem. Mater. **29**, 10496 (2017).
[11] Y. Wang, W. D. Richards, S.-H. Bo, L. J. Miara, and G. Ceder, Chem. Mater. **29**, 7475 (2017).
[12] D. A. Weber, A. Senyshyn, K. S. Weldert, S. Wenzel, W. Zhang, R. Kaiser, S. Berendts, J. Janek, and W. G. Zeier, Chem. Mater. **28**, 5905 (2016).
[13] Z. Zhu, I.-H. Chu, and S. P. Ong, Chem. Mater. **29**, 2474 (2017).
[14] N. Kamaya *et al.*, Nat. Mater. **10**, 682 (2011).
[15] B. Singh, M. K. Gupta, R. Mittal, and S. L. Chaplot, J. Mater. Chem. A **6**, 5052 (2018).
[16] Z. Wang, H. Xu, M. Xuan, and G. Shao, J. Mater. Chem. A **6**, 73 (2018).
[17] X. He, Y. Zhu, and Y. Mo, Nat. Commun. **8**, 15893 (2017).
[18] X. Wang, R. Xiao, H. Li, and L. Chen, Phys. Rev. Lett. **118**, 195901 (2017).
[19] J. R. Nelson, R. J. Needs, and C. J. Pickard, Phys. Rev. B **98**, 186102 (2018).
[20] N. Nitta, F. Wu, J. T. Lee, and G. Yushin, Mater. Today **18**, 252 (2015).
[21] J. B. Goodenough and K.-S. Park, J. Am. Chem. Soc. **135**, 1167 (2013).
[22] J.-M. Tarascon, Phys. Eng. Sci. **368**, 3227 (2010).
[23] F. Altorfer, W. Bührer, I. Anderson, O. Schärpf, H. Bill, P. L. Carron, and H. G. Smith, Physica B **180–181**, 795 (1992).
[24] T. W. D. Farley, W. Hayes, S. Hull, M. T. Hutchings, M. Alba, and M. Vrtis, Physica B **156–157**, 99 (1989).
[25] V. Thangadurai, S. Narayanan, and D. Pinzaru, Chem. Soc. Rev. **43**, 4714 (2014).
[26] U. V. Alpen, E. Schönherr, H. Schulz, and G. H. Talat, Electrochim. Acta **22**, 805 (1977).
[27] S. Kirklin, B. Meredig, and C. Wolverton, Advanced Energy Materials **3**, 252 (2013).
[28] M. D. Bhatt and C. O'Dwyer, Physical Chemistry Chemical Physics **17**, 4799 (2015).
[29] G. K. Phani Dathar, J. Balachandran, P. R. C. Kent, A. J. Rondinone, and P. Ganesh, J. Mater. Chem. A **5**, 1153 (2017).
[30] J. B. Goodenough, H. Y. P. Hong, and J. A. Kafalas, Mater. Res. Bull. **11**, 203 (1976).
[31] H. Park, K. Jung, M. Nezafati, C.-S. Kim, and B. Kang, ACS Applied Materials & Interfaces **8**, 27814 (2016).
[32] K. Wakamura, Phys. Rev. B **59**, 3560 (1999).
[33] M. K. Gupta, P. Goel, R. Mittal, N. Choudhury, and S. L. Chaplot, Phys. Rev. B **85**, 184304 (2012).
[34] P. Goel, M. K. Gupta, R. Mittal, S. Rols, S. J. Patwe, S. N. Achary, A. K. Tyagi, and S. L. Chaplot, J. Mater. Chem. A **2**, 14729 (2014).
[35] H. Fang and P. Jena, ACS Appl. Mater. Interfaces **11**, 963 (2019).
[36] X. Judez, H. Zhang, C. Li, G. G. Eshetu, J. A. González-Marcos, M. Armand, and L. M. Rodriguez-Martinez, J. Electrochem. Soc. **165**, A6008 (2018).
[37] F. Zheng, M. Kotobuki, S. Song, M. O. Lai, and L. Lu, J. Power Sources **389**, 198 (2018).
[38] O. Pecher, J. Carretero-González, K. J. Griffith, and C. P. Grey, Chem. Mater **29**, 213 (2017).
[39] C. P. Grey and N. Dupré, Chem. Rev. **104**, 4493 (2004).
[40] D. Wiedemann, S. Indris, M. Meven, B. Pedersen, H. Boysen, R. Uecker, P. Heitjans, and M. Lerch, Zeitschrift für Kristallographie-Crystalline Materials **231**, 189 (2016).
[41] J. Bréger, N. Dupré, P. J. Chupas, P. L. Lee, T. Proffen, J. B. Parise, and C. P. Grey, J. Am. Chem. Soc. **127**, 7529 (2005).
[42] J. Yang and J. S. Tse, Comput. Mater. Sci. **107**, 134 (2015).
[43] Y. Kato, S. Hori, T. Saito, K. Suzuki, M. Hirayama, A. Mitsui, M. Yonemura, H. Iba, and R. Kanno, Nature Energy **1**, 16030 (2016).
[44] E. Kendrick, J. Kendrick, K. S. Knight, M. S. Islam, and P. R. Slater, Nat. Mater. **6**, 871 (2007).
[45] T. W. D. Farley, W. Hayes, S. Hull, M. T. Hutchings, and M. Vrtis, J. Phys. Condens. Matter **3**, 4761 (1991).
[46] F. Kubel, B. Bertheville, and H. Bill, Zeitschrift für Kristallographie-New Crystal Structures **214**, 302 (1999).
[47] A. Lazicki, C.-S. Yoo, W. J. Evans, and W. E. Pickett, Phys. Rev. B **73**, 184120 (2006).
[48] O. I. Barkalov, P. G. Naumov, C. Felser, and S. A. Medvedev, Solid State Sci. **61**, 220 (2016).
[49] H. Tsukasaki, S. Mori, H. Morimoto, A. Hayashi, and M. Tatsumisago, Sci. Rep. **7**, 4142 (2017).
[50] M. Tatsumisago, M. Nagao, and A. Hayashi, Journal of Asian Ceramic Societies **1**, 17 (2013).
[51] H.-L. Wu, L. A. Huff, and A. A. Gewirth, ACS Applied Materials & Interfaces **7**, 1709 (2015).
[52] K. S. D. L. Price, *Neutron Scattering* (Academic Press, Orlando, 1986).
[53] J. M. Carpenter and D. L. Price, Phys. Rev. Lett. **54**, 441 (1985).
[54] S. Rols, H. Jobic, and H. Schober, C. R. Phys. **8**, 777 (2007).
[55] V. F. Sears, Neutron News **3**, 26 (1992).
[56] G. Kresse and J. Furthmüller, Phys. Rev. B **54**, 11169 (1996).
[57] G. Kresse and D. Joubert, Phys. Rev. B **59**, 1758 (1999).
[58] H. J. Monkhorst and J. D. Pack, Phys. Rev. B **13**, 5188 (1976).
[59] A. Togo and I. Tanaka, Scr. Mater. **108**, 1 (2015).
[60] R. Mittal, M. K. Gupta, and S. L. Chaplot, Prog. Mater Sci. **92**, 360 (2018).
[61] S. P. Jand, Q. Zhang, and P. Kaghazchi, Sci. Rep. **7**, 5873 (2017).
[62] S. Nosé, J. Chem. Phys. **81**, 511 (1984).
[63] M. P. Allen and D. J. Tildesley, *Computer Simulation of Liquids* (Oxford University Press, Oxford, UK, 2017).
[64] A. V. Chadwick, K. W. Flack, J. H. Strange, and J. Harding, Solid State Ion. **28–30**, 185 (1988).
[65] J. Buckeridge, D. O. Scanlon, A. Walsh, C. R. A. Catlow, and A. A. Sokol, Phys. Rev. B **87**, 214304 (2013).
[66] C. Cazorla and D. Errandonea, Phys. Rev. Lett. **113**, 235902 (2014).
[67] J. Klarbring, N. V. Skorodumova, and S. I. Simak, Phys. Rev. B **97**, 104309 (2018).

[68] J. R. Nelson, R. J. Needs, and C. J. Pickard, Phys. Rev. B **95**, 054118 (2017).
[69] C. Cazorla and D. Errandonea, Phys. Rev. B **98**, 186101 (2018).
[70] C. Cazorla, A. K. Sagotra, M. King, and D. Errandonea, J. Phys. Chem. C **122**, 1267 (2018).
[71] W. Buehrer, F. Altorfer, J. Mesot, H. Bill, P. Carron, and H. Smith, J. Phys. Condens. Matter **3**, 1055 (1991).
[72] T. W. D. Farley, W. Hayes, S. Hull, R. Ward, M. T. Hutchings, and M. Alba, Solid State Ion. **28–30**, 189 (1988).
[73] A. K. Sagotra, D. Chu, and C. Cazorla, Phys. Rev. Mater. **3**, 035405 (2019).
[74] T. Kurasawa, T. Takahashi, K. Noda, H. Takeshita, S. Nasu, and H. Watanabe, J. Nucl. Mater. **107**, 334 (1982).
[75] B. Bertheville, H. Bill, and H. Hagemann, J. Phys. Condens. Matter **10**, 2155 (1998).
[76] S. Filippov, J. Klarbring, U. Häussermann, and S. I. Simak, Phys. Rev. Mater. **3**, 023602 (2019).
[77] Y. Oishi, Y. Kamei, M. Akiyama, and T. Yanagi, J. Nucl. Mater. **87**, 341 (1979).
[78] S. Muy *et al.*, Energy & Environmental Science **11**, 850 (2018).